A quasi-geostrophic wavelet-spectrum model for barotropic atmosphere and its numerical solution*

DAI Xingang[1,2**], WANG Ping[3] and CHOU Jifan[2]

(1. Key Laboratory of Regional Climate-Environment for Temperate East Asia, Institute of Atmospheric Physics, Chinese Academy of Sciences, START Regional Center for Temperate East Asia, Beijing 100029, China; 2. Department of Atmospheric Sciences, Lanzhou University, Lanzhou 730000, China; 3. College of Physics, Peking University, Beijing 100871, China)

Received March 11, 2004; revised April 14, 2004

Abstract A quasi-geostrophic wavelet-spectrum model of barotropic atmosphere has been constructed by wavelet-Galerkin method with the periodic orthogonal wavelet bases. In this study a wavelet grid-spectrum transform method is designed to decrease the tremendous computation of the nonlinear interaction term in the model, and a two-dimensional Helmholtz equation from the model in a wavelet spectrum form is derived, and a solution with high precision under the periodic boundary condition is obtained. The numerical investigation manifests that the wavelet-spectrum model (WSM) could keep on running for a long time under the forcing of heating and topography. Although its numerical solution is compatible with the grid model (GM), the WSM is of a higher precision and faster convergence rate than GM's. A stationary solution comes forth when the model is forced only by the surface heating, whereas a quasi-periodic oscillation with a period about 15 days appears as considering the topography in the model. The latter oscillation, to some extent, is very similar to the Rossby index cycle of atmosphere over middle and high latitudes.

Keywords: β-plane, barotropic atmosphere, wavelet-spectrum model, wavelet grid-spectrum transform.

One of the important strategies for understanding atmospheric general circulation is to study the numerical solution of its governing equations[1]. There are two main kinds of discrete models, i.e. spectrum model and grid model. The latter employs the finite difference approximation and easily fits a complex boundary condition. But it is insufficient to represent a continuous function. The atmospheric waves simulated with the grid model usually propagate more slowly than observations. In addition, it would be in difficulty of dealing with the grids at the two poles of the earth. Besides, there exist aliasing errors in nonlinear-term computations. Fortunately, this problem is gradually overcome by a series of numerical conservation schemes designed for the finite difference approximation[2]. The spectrum model is a group of ordinary differential equations, derived from the governing equations based on some orthogonal bases. For instance, both the Fourier bases and the spherical harmonic functions are global bases, named in mathematics. The spectrum method can represent the derived terms of the equations in high precision, while for the function with discontinue or jump points, like sharp topography or rainfall that is spatially discontinued, it would cause "Gibbs phenomenon", like "minus topography" or "minus moisture" and so forth[3,4]. These problems are remarkable in the low-resolution spectrum model.

The construction of compactly supported orthogonal wavelet bases[5~7] not only is to provide a powerful tool for signal procession and compression, but also brings us some new ideas or possibilities for numerical solution of partial differential equations[8]. Since some of the wavelet bases are compactly supported in both physical and spectrum spaces, the reconstruction errors of a function are usually limited around the sharp or jump points[3]. Moreover, there is a high compression rate and reconstruction rate in signal representation if the wavelet bases are used. Owing to these advantages the wavelet bases have been used in numerical solution of differential equations in several ways, like wavelet-Galerkin method[8,9], wavelet collocation[10] and WOFD[11], for example. In fact, they already succeeded in simulating the propagation of discontinuity in fluid[8], viscoelastic plume-lithosphere interaction[10] and Kelvin wave in the tropical Pacific[11]. These examples imply a great availability of wavelet methods in numerical solution of differential equations.

* Supported by the National Natural Science Foundation of China (Grant No. 49875024) and the Major State Basic Research Development Program of China (G1999043400)

** To whom correspondence should be addressed. E-mail: daixg@lzu.edu.cn

Nevertheless, it is hard to find the examples of solution of vorticity equation using wavelets because it involves a high order problem and numerical solution of a Poisson equation, which is very difficult to deal with. Qian and Weiss only studied a simplified vorticity equation that includes advection and dissipation terms for uncompressible fluid and non-divergence flow[12]. This paper focuses on the numerical solution of atmospheric potential vorticity equation that includes topography, heating, divergence term, the advection and dissipation. In addition, we have to solve a Helmholtz equation, rather than a Poisson equation, for the trend of stream function.

1 Orthogonal wavelet bases

The multiresolution analysis (MRA)[13] is a general theory on construction of orthogonal wavelet bases, i.e. wavelet function $\psi(x)$ and scaling function $\varphi(x)$. They can be used to make the orthonormal wavelet bases[6,7]:

$$\varphi_{j,k}(x) = 2^{j/2}\varphi(2^j x - k), \quad \varphi_{j,k}(x) \in V_j, \tag{1}$$

$$\psi_{j,k}(x) = 2^{j/2}\psi(2^j x - k), \quad \psi_{j,k}(x) \in W_j, \tag{2}$$

where the subscript "j" is the dilation or resolution, and "k" is the shift, both belong to integer set ZZ. A close subset $\{V_j\}_{j\in ZZ}$ of MRA holds

$$\cdots \subset V_j \subset V_{j+1} \cdots \subset L^2(IR) \quad j \in ZZ. \tag{3}$$

The W_j is the orthogonal complement of V_j, and there holds

$$V_{j+1} = V_j \oplus W_j. \tag{4}$$

The scaling function $\varphi_{j,k}(x)$ is merely the orthonormal bases in subspace V_j due to a fixed resolution j, while $\psi_{j,k}(x)$ is the orthonornal bases in $L^2(IR)$ due to its dilation and shift. Their relationships read

$$\int_{-\infty}^{\infty} \varphi_{j,k}(x)\varphi_{j,l}(x)\mathrm{d}x = \delta(k-l), \tag{5}$$

$$\int_{-\infty}^{\infty} \psi_{j,k}(x)\,\psi_{m,n}(x)\mathrm{d}x = \delta(j-l)\,\delta(k-m), \tag{6}$$

$$\int_{-\infty}^{\infty} \varphi_{j,k}(x)\,\psi_{m,l}(x)\mathrm{d}x = 0, \tag{7}$$

where $\delta(x)$ is the Dirac function. However, the wavelet bases above are defined on a real line, which needs the interval wavelet bases for the solution of differential equation. Since such wavelets are still under development[14], we take the periodic wavelet bases defined in interval $[0, 1]$ as the expansion bases. The periodic wavelet can be derived by the summation of the classic wavelets (1) and (2) as[15]

$$\tilde{\varphi}_{J,k}(x) = \sum_{l\in ZZ}\varphi_{J,k}(x-l), \tag{8}$$

$$\tilde{\psi}_{j,k}(x) = \sum_{l\in ZZ}\psi_{j,k}(x-l), \tag{9}$$

where $\tilde{\varphi}_{J,k}(x)$ and $\tilde{\psi}_{j,k}(x)$ are periodic scaling function and wavelet. $\tilde{\varphi}_{J,k}(x)\in V_J$, $\tilde{\psi}_{j,k}(x)\in W_J$, and they satisfy

$$V_{J+1} = V_J \oplus W_J, \tag{10}$$

$$L^2(IR) = \mathrm{close}_{L^2(IR)}\Big(V_0 \bigoplus_{J=0}^{\infty} W_J\Big). \tag{11}$$

A square integral function can be expanded with the scaling function or wavelet bases, or both of them, of which the scaling function expansion reflects the approximation part of the function, while the wavelet expansion describes its details. To simulate the barotropic Rossby wave on low-resolution grids the scaling function $\tilde{\varphi}_{J,k}(x)$ is employed in the numerical solution of the barotropic model.

2 Barotropic model

In 1979, based on a quasi-geostrophic potential vorticity equation of the barotropic atmosphere, Charney et al.[16] developed a barotropic model that includes the adiabatic heating, friction and topography in a β-plane channel. Its non-dimensional form reads

$$\frac{\partial}{\partial t}\left(\nabla^2\psi - \frac{\psi}{\lambda^2}\right) + J(\psi, \nabla^2\psi + h) + \beta\frac{\partial\psi}{\partial x} + k\nabla^2(\psi - \psi^*) = 0, \tag{12}$$

where ψ, h, ψ^* are respectively the quasi-geostrophic stream function, the topography and the adiabatic heating stream function, and $\lambda^2 = gH/(f_0^2L^2)$, $\beta = L/a \approx 1/4$, $k = D_E/(2H)$, $\pi L = 5\times 10^6$ m, $H = 10^4$ m. $f_0 = 2\Omega\sin\phi_0$ is the Coriolis parameter, $\phi_0 = 45^\circ$N. "g" is the gravity acceleration, "a" is the earth's radius. $D_E = (2\nu_E/f_0)^{1/2}$ is the Ekman depth, where ν_E is the volume vortex viscosity coefficient. To use the periodic wavelet Eq. (12) must be defined in a unit square with periodic boundary condition as the following:

$$(\nabla^2 - \lambda_0^2)\frac{\partial\psi}{\partial t} = -J(\psi, C+h) - \beta\frac{\partial\psi}{\partial x} - k(C - C^*), \tag{13}$$

$$(x,y) \in G = \{(x,y) \mid (x,y) \in [0,1] \otimes [0,1]\},$$

$$\frac{\partial^2\psi}{\partial x^2} + \frac{\partial^2\psi}{\partial y^2} = C, \tag{14}$$

$$\psi(x,y) = \psi(x \pm n, y \pm n) \quad n \in ZZ, \tag{15}$$

where $\lambda_0^2 = \lambda^{-2}$, $C^* = \nabla^2\psi^*$, $k = 0.01$. Eqs. (13)

~(15) are the non-dimensional barotropic model in a β-plane channel, by which we deal with the wavelet method in the rest of the paper.

3 Wavelet spectrum model

If stream function $\Psi(x, y)$ ($\in L^2(IR)$) is a 1-period function, map it onto the subspace V_J and get its approximate expansion at resolution J as

$$\begin{aligned}\psi(x, y) &= P_{V_J}(\Psi(x, y)) \\ &= \sum_{i=0}^{2^J-1}\sum_{k=0}^{2^J-1}\psi_{J, i, k}\varphi_{J, i}(x)\varphi_{J, k}(y), \end{aligned} \tag{16}$$

where P_{V_J} is an orthogonal mapping operator, and the expansion coefficients are defined as

$$\psi_{J, i, k} = \iint_G \Psi(x, y)\varphi_{J, i}(x)\varphi_{J, k}(y)\mathrm{d}x\mathrm{d}y. \tag{17}$$

$J \to \infty$, so $\psi(x, y) \to \Psi(x, y)$. Similarly, the derivates of the stream function are expanded to

$$\begin{aligned}\frac{\partial\psi}{\partial x} &\approx P_{V_J}\left(\frac{\partial\psi}{\partial x}\right) \\ &= \sum_{j=0}^{2^J-1}\sum_{k=0}^{2^J-1} CX_{J, j, k}\varphi_{J, j}(x)\varphi_{J, k}(y), \end{aligned} \tag{18}$$

$$\begin{aligned}\frac{\partial^2\psi}{\partial x^2} &\approx P_{V_J}\left(\frac{\partial^2\psi}{\partial x^2}\right) \\ &= \sum_{j=0}^{2^J-1}\sum_{k=0}^{2^J-1} CXX_{J, j, k}\varphi_{J, j}(x)\varphi_{J, k}(y), \end{aligned} \tag{19}$$

where the expansion coefficient of (18) is

$$CX_{J, j, k} = \iint_G \frac{\partial\psi}{\partial x}\varphi_{J, j}(x)\varphi_{J, k}(y)\mathrm{d}x\mathrm{d}y. \tag{20}$$

Substituting (16) into (20), and making a series of mathematical transformations, we get

$$\begin{aligned}CX_{J, j, k} = 2^J &\sum_{l=0}^{2^J-1}\sum_{m=0}^{2^J-1}\psi_{J, l, m}\int\varphi_{l-j}^{(1)}(x)\varphi(x)\mathrm{d}x \\ &\cdot\int\varphi(y-m)\varphi(y-k)\mathrm{d}y, \end{aligned} \tag{21}$$

where the superscript "(1)" represents the derive order 1, and "$l-j$" is the shift. Notice the support and periodicity of the scaling function, equality (21) yields

$$CX_{J, j, k} = 2^J\sum_{l=2-ND}^{ND-2}\psi_{J, l+j, k}\Omega_l^1, \tag{22}$$

where ND is the Daubechies genus, and the definition of 2-term connection coefficients is

$$\Omega_i^1 = \int\varphi(x)\varphi_i^{(1)}(x)\mathrm{d}x. \tag{23}$$

Using a similar mathematic operation we get the scaling function transform (SFT) of the stream function derivate in second order, which reads

$$CXX_{J, j, k} = 2^{2J}\sum_{l=2-ND}^{ND-2}\psi_{J, l+j}\Omega_l^2, \tag{24}$$

where the 2-term connection coefficient is defined as the following:

$$\Omega_i^2 = \int\varphi(x)\varphi_i^{(2)}(x)\mathrm{d}x. \tag{25}$$

Besides, it is very easy to get the SFT of its vorticity $C_{J, j, k}$ (or noted as $C_J(j, k)$) by equality (24). As the 2-term connection coefficients could be precisely calculated by an algebraic technique developed by Dahmen et al.[17], the wavelet-represented derivates are very accurate or have very small truncation errors in numerical computation.

We expand ψ, ψ^* and vorticity-advection term (including the topography) with the periodic scaling function, and substitute them into Eq. (13), and then multiply each side of the equation by $\varphi_{J, p}(x)\varphi_{J, q}(y)$. Furthermore, notice the orthogonal property of the scaling functions and (16) ~ (25), we make an integration over $\boldsymbol{G}$ on the two sides of the equation and finally get the barotropic potential equation or model in the wavelet-spectrum form:

$$(C_J(p, q))_t - \lambda_0^2(\psi(p, q))_t = -F_J(p, q), \tag{26}$$

where

$$\begin{aligned}F_J(p, q) = H_J(p, q) &+ 2^J\beta\sum_{l=2-ND}^{ND-2}\psi(l+p, q)\Omega_l^1 \\ &- k(C_J(p, q) - C_J^*(p, q)) = 0, \end{aligned} \tag{27}$$

$$H_J(p, q) = \iint_G J(\psi, C+h)\varphi_{J, p}(x)\varphi_{J, q}(y)\mathrm{d}x\mathrm{d}y. \tag{28}$$

As a similar case in triangular bases or spherical harmonic bases the calculation of the $H_J(p, q)$ is a too big job to deal with. Thus, one cannot calculate it directly, and instead, to overcome this difficulty we design a wavelet grid-spectrum transform method which will be presented in the next section.

Eq. (26) is a Helmholtz equation about the trend of the stream function. It can be rewritten in the following form:

$$\begin{aligned}\sum_{l=2-ND}^{ND-2}(\psi_t)_{J, l+p, q}\Omega_l^2 &+ \sum_{m=2-ND}^{ND-2}(\psi_t)_{J, p, m+q}\Omega_m^2 \\ &- 2^{-2J}\lambda_0^2(\psi_t)_{p, q} = -2^{-2J}F_J(p, q). \end{aligned} \tag{29}$$

Under the periodic condition Eq. (29) can be transformed into a matrix algebraic equation

$$\Omega\Psi_t + \Psi_t\Omega = -2^{-2J}\boldsymbol{F}, \tag{30}$$

where matrix Ω is a circulant matrix made by wavelet connection coefficients Ω_i^2, i.e.

$$\Omega = \mathrm{circ}(\Omega_0^2 - 2^{-2J-1}\lambda_0^2, \Omega_1^2, \Omega_2^2, \cdots, \Omega_{ND-2}^2, 0\cdots0, \Omega_{2-ND}^2, \cdots, \Omega_{-2}^2, \Omega_{-1}^2). \tag{31}$$

4 Numerical schemes

4.1 Wavelet grid-spectrum transform

Given heating $\boldsymbol{C}^*$ and the periodic boundary condition, we can get the numerical solution ($\psi(p, q)$) by the wavelet spectrum model through integration of Eqs. (26) and (29). And then its inverse transform gives the solution of the stream function $\psi(x, y)$ in physical space. How to reduce the computation burden of $H_J(p, q)$ is the key problem for the integration because it is a nonlinear interaction term, whose calculation is almost impossible for an extensive calculation. So, we have to turn to design a wavelet grid-spectrum transform method for calculating $H_J(p, q)$. It includes the following four steps: (i) calculate the SFT of the stream function and vorticity in wave-number space; (ii) make an inverse SFT to them and get their derivates in physical space; (iii) calculate the vorticity advection and topography terms in physical space by multiplication; (iv) make an SFT to the sum of the two terms and substitute them into (26) to joint time integration.

The numerical exercises show that the wavelet grid-spectrum method can sharply decrease the computation quantity, and the model integration is fast and stable.

4.2 Helmholtz equation

The solution of Eq. (30) can be obtained by an algebraic method[12]. The circulant matrix Ω is decomposed by FFT as

$$\Omega = \Phi\boldsymbol{D}_\Omega\Phi^{\mathrm{T}}, \tag{32}$$

where matrix Φ is the eigenvectors of the matrix Ω, $\Phi\Phi^{\mathrm{t}} = \boldsymbol{I}$ and $\boldsymbol{D}_\Omega = \mathrm{diag}\{\lambda_i\}$, where λ_i ($i = 1, 2, \cdots, N$) is the eigenvalues of the matrix Ω. With Eq. (32) and some algebraic transforms the solution of (30) can be given as

$$\Psi_t = -2^{-2J}\Phi(\boldsymbol{B}_\Omega \,.\backslash (\Phi^{\mathrm{t}}\boldsymbol{F}\Phi))\Phi^{\mathrm{t}}, \tag{33}$$

where

$$\boldsymbol{B}_\Omega = \boldsymbol{D}_\Omega\begin{pmatrix} 1 & \circ & \circ & 1 \\ \circ & \circ & \circ & \circ \\ \circ & \circ & \circ & \circ \\ 1 & \circ & \circ & 1 \end{pmatrix} + \begin{pmatrix} 1 & \circ & \circ & 1 \\ \circ & \circ & \circ & \circ \\ \circ & \circ & \circ & \circ \\ 1 & \circ & \circ & 1 \end{pmatrix}\boldsymbol{D}_\Omega \tag{34}$$

and ".\" in (33) is a matrix element-to-element division operator. Numerical investigation reveals that it would produce very large errors if FFT decomposition is applied to matrix Ω. Instead, we employ Jacobian decomposition to calculate its eigenvalues and eigenvectors.

Integrate Eq. (33) and get the stream function SFT, with which the vorticity SFT reads

$$\boldsymbol{C} = 2^{2J}(\Omega^*\Psi + \Psi\Omega^*), \tag{35}$$

where Ω^* is also a circulant matrix defined as

$$\Omega^* = \mathrm{circ}(\Omega_0^2, \Omega_1^2, \Omega_2^2, \cdots, \Omega_{ND-2}^2, 0\cdots0, \Omega_{2-ND}^2, \cdots, \Omega_{-2}^2, \Omega_{-1}^2). \tag{36}$$

In the following computation we employ Daubechies periodic wavelet Daub10 ($ND = 10$). There are 16×16 grids on a unit square $\boldsymbol{G}$, equivalent to resolution of $J=4$.

5 Numerical results

5.1 Heat-forcing circulation

Let $h(x, y) = 0$, i.e. there is no topography. To fit the periodic boundary condition the heat forcing is of a little difference to that of Charney's model. Set the heating function as

$$C^*(x, y) = -0.24\sqrt{2}\sin(2\pi y) - 0.4\cos(2\pi x)\sin(2\pi y). \tag{37}$$

The initial field reads

$$\psi(x, y) = 0.01\cos(2\pi x)\sin(2\pi y). \tag{38}$$

The time integration used is Runge-Kutta scheme in order 4, with a time step 0.27, equivalent to 1/32 day. We run the model for 32000 steps, equal to 1000 days on computer SGI-2100. In order to observe the evolution of the numerical solution we define a zonal circulation index as the following:

$$I_R = \sum_{i=1}^{16}[\psi(i, 7) - \psi(i, 11)]. \tag{39}$$

The numerical results showed that I_R rapidly converges into a stationary solution after it experienced a short-period oscillation (Fig. 1 (a)). The output field of the non-dimensional stream function at the last step shows two lows or cyclones in the north, and two highs or anticyclones in the south (Fig. 1 (c)), which is allocated with the heat forcing.

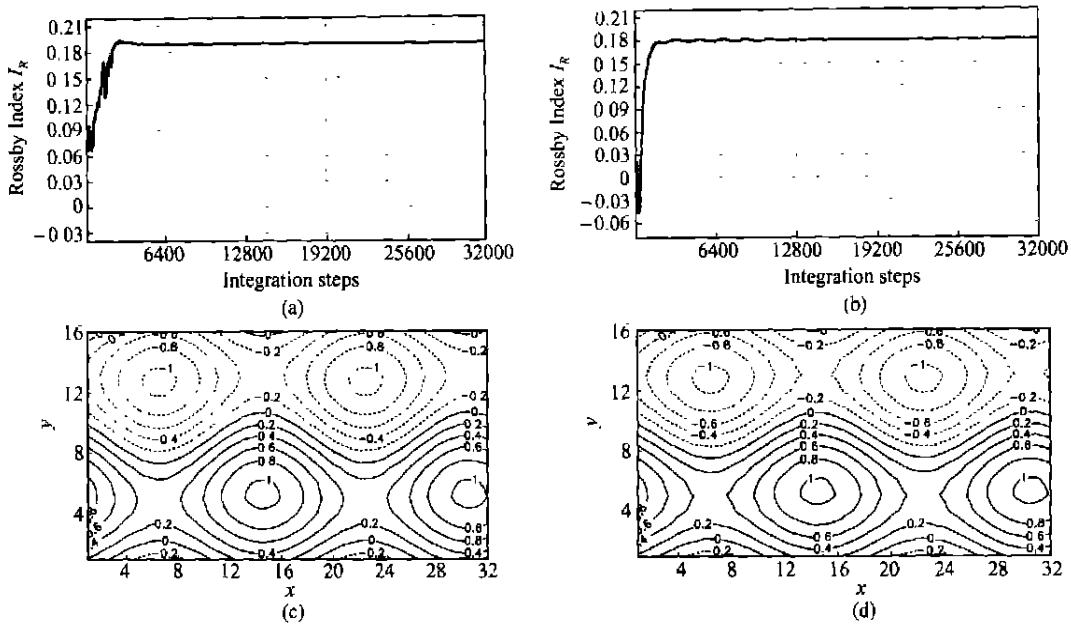

Fig. 1. Evolution of simulated zonal circulation index I_R and the non-dimensional stream function at the last step. (a) and (c), Wavelet spectrum model; (b) and (d), grid model (unit: 0.012).

To confirm the model construction and mathematic operation we solve the models (13) ~ (15) by finite difference approximation under the same heat forcing and the boundary condition. The Helmholtz equation (13) is solved by the numerical iteration method[4] with a threshold 10^{-6}. Arakawa quadrature conservation scheme[2] in a precision order 4 is employed to discrete the vorticity advection term. The time integration scheme is the same with the wavelet model. The convergence field of the stream function for the grid model is almost the same as the wavelet model (see Fig. 1 (d)), and the I_R for wavelet model is slightly higher than the grid one (Fig. 1 (b)). And the solution convergence rate of the wavelet model is faster than the grid model. An ideal numerical investigation on the solution of the Helmholtz equation shows that the precision of wavelet-Galerkin method is ten times higher than the difference method. Moreover, one can get a precise solution of a differential equation using wavelet-Galerkin method if wavelet interpolation in its inverse SFT is employed.

5.2 Topography-forced circulation

The Rossby index cycle is one of the most important non-linear characteristics of atmospheric circulation in middle and high latitudes. The high index corresponds to an intensive zonal circulation, whereas the low one represents a weak zonal one or the one with high amplitudes. The Charney's model does succeed in reproducing an oscillation in a period about 15 days. Notice the model integration domain $\boldsymbol{G}$ and the grid displace (1/16), smaller than Charney's mode ($\pi/16$). For preventing sharp topography gradient we take $h(x, y)$ to be the same as Charney's model, but cut a half of its amplitude. In addition, the minus part of the function $h(x, y)$ has been set to zero. It becomes

$$h(x,y) = \begin{cases} 0.1\cos(2\pi x)\sin(\pi y) & (x,y)\in D=\{(x,y)\mid h>0\}, \\ 0 & \text{otherwise.} \end{cases} \tag{40}$$

Considering the periodic boundary condition, the heating function reads

$$C^*(x,y) = -0.2\sqrt{2}\sin(2\pi y). \tag{41}$$

Running the wavelet model and the grid model for 1000 days with a time step $\Delta t = 0.27$ and initial field (32), we get a quasi-periodic solution like the index cycle for the model (Fig. 2 (a)), in which the 200-day points of the index I_R from the beginning are cut off due to its spin-up process. There are two significant periods, i.e. 15 days and 30 days (Fig. 2 (b), (c)) according to the Morlet wavelet power spectrum of the Index sequence[18], the latter period is significant only during 300 ~ 500 days. The areas circled by the white curve in Fig. 2 (b) represent the statistical significance level above 0.05. The global wavelet spectrum is shown in Fig. 2 (c), where the dashed

line is its significance level at 0.05.

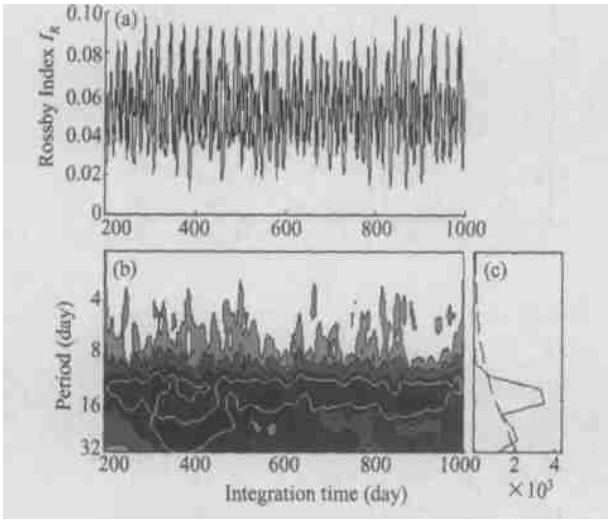

Fig. 2. Simulated Rossby index cycle and its wavelet power spectrum. (a) Index I_R; (b) Morlet wavelet power spectrum; (c) global wavelet spectrum, where the white lines in (b) and the dashed line in (c) represent statistical significance at 0.05.

Under the same heat forcing, topography and initial field as a wavelet model we run the grid model for 1000 days and get a similar quasi-periodic oscillation solution (Fig. 3 (a)). There are also the periods of 15 days and 30 days in its Morlet wavelet power spectrum (Fig. 3 (b)). Comparing Fig. 2 with Fig. 3 one can find the difference between them. Firstly, there exists more high frequency oscillation with periods shorter than 5 d for the wavelet model (Fig. 2 (b), Fig. 3 (b)), while the energy is more concentrated on the components of 15-day and 30-day periods for the grid model. The latter is more significant than that for the wavelet model. This manifests that the Arakawa conservation scheme can depress the generation of short waves during the model integration. A further numerical investigation confirms that the maximum time step for running the wavelet model is usually shorter than the grid model. This implies the necessity to study how to improve the computational stability for the wavelet model.

The indices of both models evolve like a similar quasi-periodic oscillation and their flow patterns are also very close. We choose two points in the high indices at steps 27552 (Fig. 2 (a)) and 26957 (Fig. 3 (b)), and two points in the low indices at steps 27812 (Fig. 2 (a)) and 27233 (Fig. 3 (b)), respectively and contour their stream function fields (Fig. 4). The similarity of their flow patterns at the high or low indices manifests the availability of the wavelet model on simulating the nonlinear characteristics of the barotropic atmosphere.

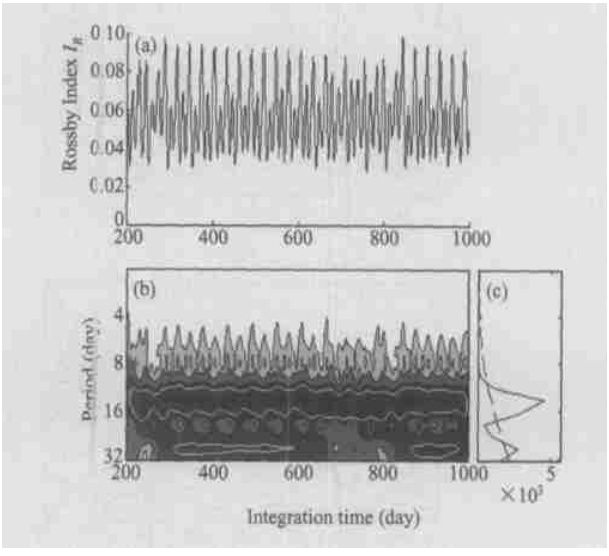

Fig. 3. Evolution of the Index I_R and its wavelet power spectrum for the grid model, others the same as in Fig. 2.

6 Conclusion and discussion

The quasi-geostrophic wavelet spectrum model for the barotropic atmosphere in a β-plane channel has been built by wavelet-Galerkin method. To avoid the tremendous computation of the vorticity advection, we developed a wavelet grid-spectrum transform method that replaces a direct computation with the nonlinear interaction term. It overcomes one of the key difficulties about the wavelet spectrum application in the climate model or the general circulation model of atmosphere. The numerical solution of a two-dimensional Helmholtz equation is another difficult problem for the wavelet model because of its high order derivates. Among several matrix decompositions the Jacobian method is of the highest precision for the solution of the equation. Its precision is much higher than the iteration method when the finite difference approximates are employed, and it needs much less computation. Under the same boundary condition and forcing the solutions of the wavelet and grid model are very close, which confirms the mathematical operations and numerical schemes of the wavelet model construction. The wavelet model cannot only simulate the stationary solution under the heat forcing, but also produce an oscillation solution like the Rossby index cycle. It implies the potential capacity of the wavelet method in simulation of large-scale nonlinear motion of atmosphere.

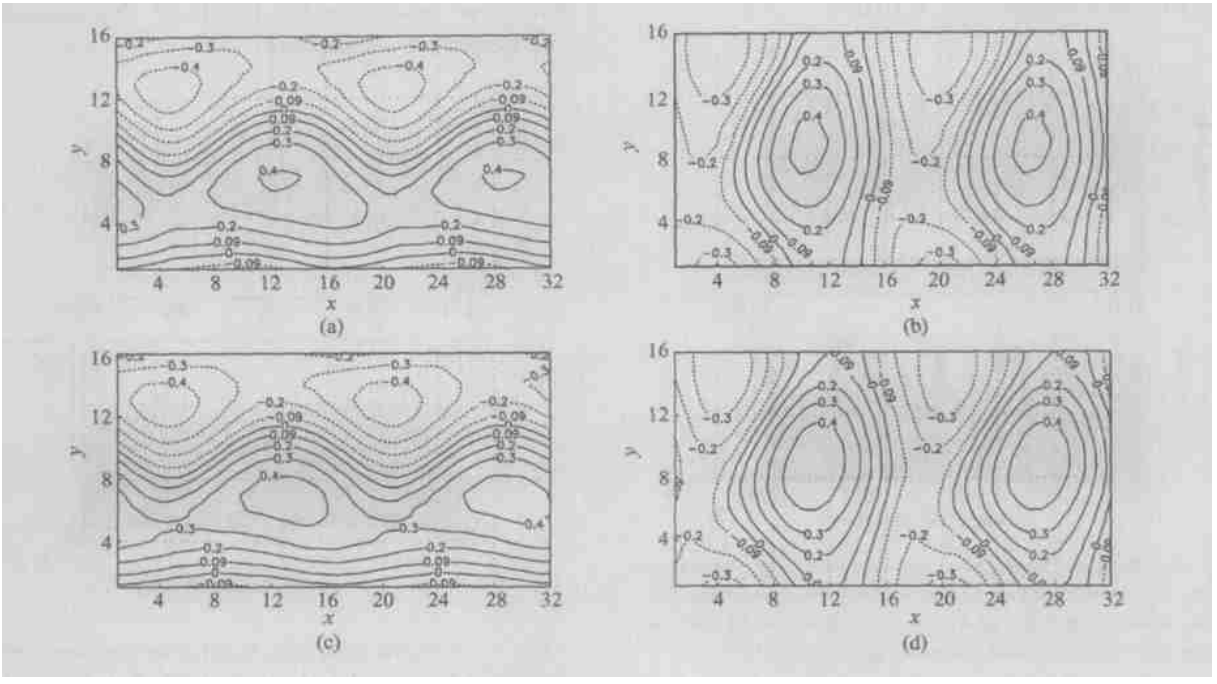

Fig. 4. The stream function patterns correspond to two high indices and two low Indices for the wavelet model and grid model, respectively. (a) High index (I_R= 0.0876) for wavelet model; (b) high Index (I_R= 0.0999) for grid model; (c) low index (I_R= 0.0133) for wavelet model; (d) low index (I_R= 0.0133) for grid model, where the values in the figure have been multiplied by 1000.

Obviously, the construction and successful running of the wavelet spectrum model in a β-plane channel is one of the important steps for developing a more complex wavelet spectrum model of atmosphere. But there is still a lot to do for construction of spherical wavelet spectrum model with the wavelet-Galerkin technique.

Acknowledgement We are very grateful to Dr. J. Weiss, Dr. A. Fournier and Professor J. Antoine for their encouragement and kind help on numerical computation. We also express our sincere thanks to Dr. C. Torrence for his wavelet analysis code and valuable discussion.

References

1 Chang, J. General Circulation Models of Atmosphere. New York: Academic Press, 1977.
2 Arakawa, A. Computational design for long-term numerical integration of the equations of fluid motion: two-dmensional incompressible flow. Part I. J. Comp. Phys., 1966, 1: 119.
3 Dai, X. G. et al. Two-dimensional wavelet transform and its application in topography expansion of Tibetan Plateau. Chinese J. Comp. Phys. (in Chinese), 2003, 20: 529.
4 Liao, D. X. et al. The Principle and Application of Numerical Weather Prediction (in Chinese). Beijing: Chinese Meteorological Press, 1986.
5 Chui, C. K. An Introduction to Wavelets. Boston: Academic Press, 1992.
6 Meyer, Y. Ondelettes et Operateurs (in Frech). Paris: Hermann, 1990.
7 Daubechies, I. Orthogonal bases of compactly supported wavelets. Pure App. Math., 1988, 41: 906.
8 Beylkin, G. et al. On the adaptive numerical solution of nonlinear partial differential equations in wavelet bases. J. Comp. Phys., 1997, 132: 233.
9 Restrepo, J. M. et al. Wavelet-Galerkin discretization of hybolic equations. J. Comp. Phys., 1995, 122: 118.
10 Vasilyev, O. V. et al. Modeling of viscoelastic plume-lithosphere interaction using the adaptive multilevel wavelet collocation method. Geophys. J. Int., 2001, 147: 579.
11 Jameson, L. et al. Wavelet analysis and ocean modeling: a dynamically adaptive numerical method "WOFD-AHO". Mon. Wea. Rev., 2000, 128: 1536.
12 Qian, S. et al. Wavelet-Galerkin discretization of hyperbolic equations. J. Comp. Phys., 1995, 122: 155.
13 Mallat, S. A theory for multiresolution signal decomposition: the wavelet representation. IEEE Trans. on Pattern Analysis and Machine Intelligence, 1989, 11: 674.
14 Cohen, A. et al. Wavelet on the interval and fast wavelet transformations. Appl. and Comp. Harmonic Analysis, 1993, 1: 54.
15 Daubechies, I. Ten lectures on wavelets. CBMS-NSF Series in Applied Mathematics, 61, SIAM Publications, Philadelphia, 1992.
16 Charney, J. G. et al. Multiple flow equilibria in the atmosphere and blocking. J. Atmos. Sci., 1979, 36: 1205.
17 Dahmen, W. et al. Using the refinement equation for evaluating integrals of wavelets. SIAM, J. Numer. Anal., 1993, 30: 507.
18 Torrence, C. et al. A practical guide to wavelet analysis. Bulletin of the American Meteor. Soc., 1997, 79(1): 61.